Bulletin of the Seismological Society of America, Vol. 93, No. 4, pp. 1691–1702, August 2003

Stochastic Finite-Fault Modeling of Ground Motions from the 1999 Chi-Chi, Taiwan, Earthquake: Application to Rock and Soil Sites with Implications for Nonlinear Site Response

by Zafeiria Roumelioti and Igor A. Beresnev

Abstract The stochastic method for simulating strong ground motions from finite faults is applied to the records of the 1999 Chi-Chi, Taiwan, earthquake. The method involves discretization of the fault plane into smaller subfaults, each of which is assigned an ω^2 spectrum. The contributions from all subfaults are empirically attenuated to the observation site and summed to produce the synthetic acceleration time history.

The method is initially calibrated against the data recorded at 24 rock sites, located within 7–120 km from the mainshock hypocenter and providing a broad azimuthal coverage of the fault plane. The accuracy of the simulations is quantified through the model bias, defined as the logarithm of the ratio of the observed to simulated spectrum, averaged over all stations. The calibrated model for the Chi-Chi event has a near-zero average bias in reproducing the ground motions at rock sites in the frequency range from 0.1 to 20 Hz. An unusually low value is found for the radiation-strength factor *s*, controlling the high-frequency radiation level and directly related to the maximum slip velocity on the fault, compared with the mean value found for North American earthquakes. This result reflects the observed low peak ground accelerations of the Chi-Chi mainshock and, physically, its lower-than-usual slip velocities.

The calibrated model is then used to simulate soil-site (site class D) records using the linear-response assumption. The simulated soil-site input motions are amplified by the weak-motion amplification functions, estimated by the spectral-ratio technique from available aftershock records. This analysis reveals an average reduction in strong-motion amplification to about 0.5–0.6 of that in weak motions, with an acceleration "threshold" for detectable nonlinearity near 200–300 cm/sec^2. However, the derivation of soil-site specific weak-motion amplification was limited by the amount of aftershock data available; further improvement in the quantification of nonlinear soil response during the Chi-Chi earthquake may be possible with the release of additional aftershock datasets.

Introduction

While nonlinear soil response to strong earthquake motions was considered nearly hypothetical a decade ago (e.g., Aki, 1993; Beresnev and Wen, 1996; Field *et al.*, 1998a), seismological observations of the last several years have provided corroborating evidence for its significance during large events (Field *et al.*, 1997; Beresnev *et al.*, 1998a,b; Field *et al.*, 1998b; Hartzell, 1998; Su *et al.*, 1998; Cultrera *et al.*, 1999; Dimitriu *et al.*, 2000; Beresnev, 2002; Dimitriu, 2002). Within the context of seismic-hazard analysis, nonlinear soil response is typically defined as the decrease in near-surface amplification of seismic waves as their amplitude increases. This phenomenon is believed to be caused by an increasingly hysteretic character of the stress-strain relationship in soils as strain increases. At low strain, the relationship is essentially linear (e.g., Beresnev and Wen, 1996; Ishihara, 1996).

Most of the recent nonlinearity observations have come from the analysis of the 1994 Northridge, California, earthquake, recorded by a dense network of strong-motion instrumentation within and in the vicinity of the Los Angeles basin. Further investigations of the patterns of nonlinear site effect are needed to make proper generalizations; they are

naturally limited by the paucity of large events that would be recorded by dense networks of instruments. The vast strong-motion database collected during the *M* 7.6, 1999 September Chi-Chi, Taiwan, mainshock, which triggered about 441 strong-motion instruments (Lee *et al.*, 2001b), lends itself to this type of analysis.

Method

Our goal is to analyze nonlinear amplification during the Chi-Chi event by comparing the islandwide amplification observed during the mainshock with that predicted using an assumption of linear response. The detection of nonlinear site amplification may be approached in a variety of ways; in this study, we employ the method used by Beresnev *et al.* (1998a) and Beresnev (2002), based on finite-fault modeling of mainshock records and its ability to provide a statistically reliable model of rock-station data over a wide range of distances from the fault (e.g., Silva *et al.*, 1997). The method consists of two steps. Model validation is the first step of the analysis. We use the stochastic finite-fault technique to simulate the observed records of the Chi-Chi mainshock at rock sites, to see whether the model is capable of reproducing the strong-motion data recorded during this significant, well-recorded event in a complex tectonic setting with near-zero bias. The bias is defined as the logarithm of the ratio of the observed to simulated Fourier spectra, averaged over all rock sites. The rock sites are those categorized as U.S. National Earthquake Hazards Reduction Program (NEHRP) site class B ("rock") (Lee *et al.*, 2001a). NEHRP site class A ("hard rock") stations have so far not been identified in Taiwan. The finite-fault simulation code FINSIM (Beresnev and Atkinson, 1998a) is used for validation; its applicability to ground-motion prediction in various tectonic environments has been verified in several recent studies (Hartzell *et al.*, 1999; Berardi *et al.*, 2000; Castro *et al.*, 2001; Beresnev and Atkinson, 2002; Hough *et al.*, 2002; Iglesias *et al.*, 2002; Roumelioti and Kiratzi, 2002; Erdik and Durukal, 2003; Singh *et al.*, 2003). The validation for the Chi-Chi event is another test of the applicability of the stochastic method.

The second step applies the calibrated model to the simulation of soil records (site class D, "stiff soil"), with the exception that the predicted motions are amplified by the soil-response functions derived from the linear-response analyses. The prediction bias is again calculated as the logarithm of the ratio between the observed and simulated Fourier spectra, averaged over all soil sites. This bias is an estimate of the ratio of strong- to weak-motion amplification (equation 1 of Beresnev, 2002). Before averaging, each ratio is normalized by the mean prediction bias for rock sites (which should be close to unity for a well-calibrated model) to remove residual calibration error from the soil-site simulations. If the amplification during the mainshock were equal to the weak-motion amplification, the mean logarithmic soil-site prediction bias would statistically be equal to zero. However, if the bias fell below zero in a statistically significant sense, the simulated spectra then exceeded the observed spectra because the observed amplification was reduced by nonlinear soil response.

Ideally, the site-specific weak-motion amplifications should be used in generating the simulated Fourier spectra in the second step. This approach was taken by Beresnev *et al.* (1998a) and Field *et al.* (1998b). We deduce these amplifications from aftershock records obtained at soil stations that also recorded the mainshock, provided these aftershocks have also been recorded at a nearby rock site. The amplifications are then calculated using spectral ratios. We focus on site class D amplifications in this study, since pairs of nearby rock and site class E stations, which would have recorded a sufficient number of aftershocks, were not found in the available aftershock datasets.

In the following, we test the ability of the stochastic finite-fault model to simulate the records of the Chi-Chi event at rock sites and then study the possibility of using this model to detect nonlinear soil response (site class D) during the mainshock with the aftershock data currently available.

Data

The strong-motion data for the Chi-Chi mainshock were taken from the files disseminated on CD-ROM by Lee *et al.* (2001b). As stated earlier, the data used to validate the stochastic method consisted of the records at site class B, which included limestone, igneous or metamorphic rocks, hard volcanic deposits, and Miocene or older strata (sandstones, shales, conglomerates, and slates) (Lee *et al.*, 2001a).

In order to enhance azimuthal coverage of the observation stations around the seismogenic fault, we have also included site class C* in the validation. Generally, site class C of Lee *et al.* (2001a) ("very dense soil and soft rock") is chosen to be comparable to NEHRP site class C. The difference between site classes C and C* is that the latter are "borderline" stations that might be closer to site classes B or D; we therefore included those stations that exhibited surface geology characteristics close to site class B.

In the database of Lee *et al.* (2001b), the records are classified into four categories based on quality. A-quality records are the best, B-quality records may include absolute time errors, C-quality records may not have adequate pre- or postevent (traces not showing sufficient coda) data, and D-quality records have some defect (e.g., spurious spikes or a missing component). Since in the present study we are interested in the frequency content of the *S*-wave window, we used the data from the first three categories excluding only the waveforms with defects (D quality). In the cases of colocated accelerographs, we chose the recordings of the more advanced instrument (e.g., that with the largest dynamic range).

Model Validation

The locations of 24 rock stations used to validate the stochastic model are shown in Figure 1 (black triangles). Table 1 lists station information, including station-to-fault distance measures and the peak horizontal acceleration (PHA) recorded during the mainshock. Station codes and site classes are those from Lee *et al.* (2001a). As seen from Table 1, our calibration included only stations with hypocentral distances shorter than 120 km. This cutoff distance is required due to a bias in the empirical path-effect model used to generate synthetics (discussed later). Clearly, no simple model of path effect (attenuation) can describe equally well ground motions at all distances from the source. As we show later (see Fig. 5), there is no observable distance bias in the simulations in the selected distance range.

During the validation, we tested various combinations of several fault models (e.g., Wang *et al.*, 2001; Wu *et al.*, 2001; Zeng and Chen, 2001) and focal mechanisms (e.g., Chang *et al.*, 2000; Wu *et al.*, 2001) proposed in the published studies of the Chi-Chi earthquake. The combination that gave the best fit to the data was that of a rectangular fault with dimensions of 110 km $\times$ 40 km (Chi *et al.*, 2001; Ma *et al.*, 2001), a strike of 5°, and an easterly dip of 34° (Chang *et al.*, 2000). Following the approach taken by Beresnev and Atkinson (2002), the fault was assigned a homogeneous slip, since the details of the slip distribution are not well constrained and it has been found not to affect the accuracy of the predictions on average (Beresnev and Atkinson, 1998b). A study recently conducted by Beresnev (2002b) showed that only the gross features of slip distribution on a fault plane (obtained from finite-fault slip inversions) that do not diverge significantly from the average value of slip may be reliable; all other complexities could be extremely uncertain (Olson and Anderson, 1988; Das and Kostrov, 1994; Beresnev, unpublished manuscript, 2003; Delouis *et al.*, 2002). We thus find it reasonable to assume a homogeneous slip distribution instead of following the oftentimes conflicting results of published inversions (Beresnev, unpublished manuscript, 2003), considering that this approach has been properly validated (Beresnev and Atkinson, 1998b, 2002). The fault plane was discretized into 10 $\times$ 4 subfaults based on the empirical relation of Beresnev and Atkinson (2002, equation 1); the hypocenter was placed at the south-central, upper half of the fault (Chang *et al.*, 2000). The surface projection of the adopted fault model is depicted in Figure 1.

In the implementation of the stochastic method, the attenuation effects of the propagation path are modeled through the empirical Q and geometric-attenuation models. We assumed the frequency-dependent $Q = 117f^{0.77}$, estimated from coda waves by Chen *et al.* (1989), and geometric spreading in the form $1/R^b$, where $b = 1.0$ for $R < 50$ km, $b = 0$ for 50 km $\leqq R <$ 150 km, and $b = 0.5$ for $R \geqq 150$ km, which was previously used for the Taiwan region (Sokolov, 2000). Note that the adopted path-effect model satisfactorily explained data for distances less than or equal to

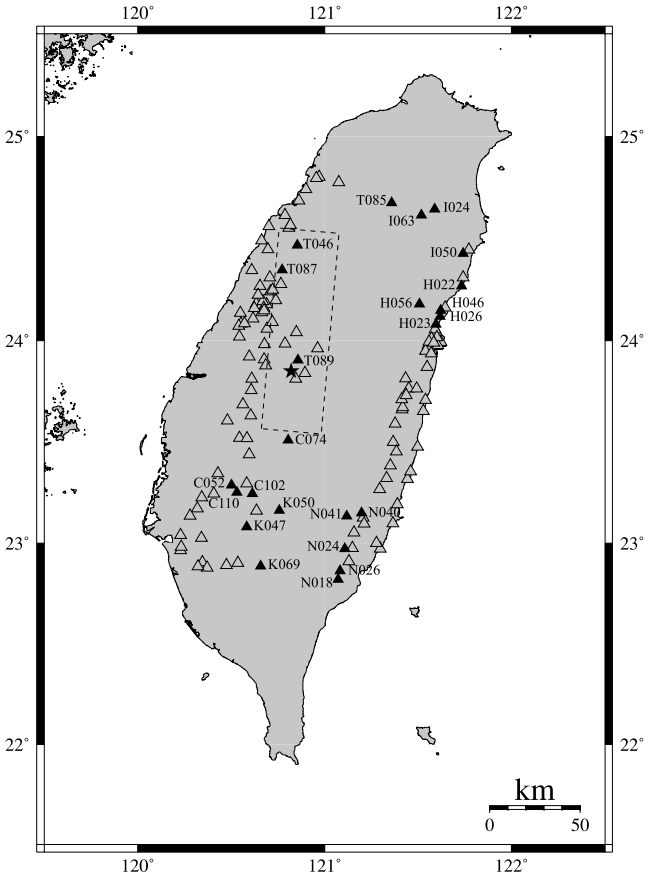

Figure 1. Regional map showing locations of rock (black triangles) and soil (gray triangles) stations used in this study. Codes are shown for rock stations. The epicenter of the 1999 Chi-Chi earthquake (star) and the surface projection of the fault plane (dashed line) are indicated.

120 km only. As discussed before, this was taken as the distance limit of our analysis. There also have been publications that introduce a distance-dependent duration term into the subevent radiation model (e.g., Ou and Herrmann, 1990). Similarly to Beresnev and Atkinson (1998b), we did not find it necessary to use the distant-dependent duration to explain acceleration time histories for the Chi-Chi mainshock and thus opted for the simpler model in which durations were equal to source durations.

The upper-crustal response was accommodated by amplifying the simulated spectra by the factors proposed for generic rock sites in western North America (Boore and Joyner, 1997). The spectra were additionally attenuated by the kappa operator (Anderson and Hough, 1984) with $\kappa = 0.07$ sec, which was the value that best fit the observed spectra.

The radiation-strength factor s, which is the parameter controlling the level of high-frequency radiation in the simulated spectra, is the only truly free parameter of the model and was determined by trial and error. Its value reflects the maximum slip velocity on the fault (Beresnev and Atkinson, 2002). The best fit within the examined frequency range

Table 1
Information on 24 Rock Stations used in Validation

Station Code	Site Class	Latitude (°)	Longitude (°)	Closest Distance to Rupture Plane (km)	Hypocentral Distance (km)	PHA (cm/sec^2)
C102	B	23.246	120.614	41.9	70.7	49
H023	B	24.080	121.596	52.0	84.6	38
H026	B	24.119	121.617	53.8	87.9	70
H046	B	24.149	121.621	54.1	89.5	84
H056	B	24.180	121.508	41.6	80.3	106
I024	B	24.645	121.588	61.5	118.2	41
I050	B	24.428	121.741	66.3	114.5	64
I063	B	24.616	121.518	54.0	111.0	92
K047	B	23.082	120.583	60.3	89.0	42
K050	B	23.163	120.757	50.3	77.4	42
K069	B	22.887	120.657	80.9	108.7	39
T046	B	24.468	120.854	16.5	67.6	140
T085	B	24.676	121.358	48.0	106.6	62
N024	B	22.973	121.108	73.0	103.3	29
N040	B	23.151	121.198	56.5	88.5	31
N041	B	23.134	121.118	56.4	86.7	79
C052	C*	23.288	120.501	41.2	70.3	151
C074	C*	23.510	120.805	14.4	38.8	229
C110	C*	23.252	120.530	43.6	72.8	28
H022	C*	24.268	121.733	64.6	105.1	119
T087	C*	24.348	120.773	3.4	54.1	119
T089	C*	23.904	120.857	8.3	7.5	348
N018	C*	22.821	121.072	88.9	118.5	35
N026	C*	22.863	121.083	84.4	114.2	38

(0.1–20 Hz) was provided by $s = 1.0$, which is lower than the average value estimated for North American earthquakes ($s = 1.5 \pm 0.3$; Beresnev and Atkinson, 2001). This result reflects the recorded low peak ground accelerations (PGAs) during the mainshock and, in physical terms, suggests a lower slip velocity than commonly observed, in agreement with other studies (e.g., Zeng and Chen, 2001; Campbell and Bozorgnia, 2003). Table 2 summarizes all parameters used in the synthetic model.

The performance of our calibrated model is demonstrated in Figure 2, where we compare the observed and simulated Fourier spectra at all 24 rock stations. Taking into account the complexity of the examined event, the simplicity of the model, and the fact that all rock-site responses were assumed to be unity, the fit can be considered very satisfactory. In Figure 3, we compare the observed and simulated acceleration time histories at six representative stations above and around the fault. In most cases, the peak values of acceleration, *S*-wave envelopes, and ground-motion durations are well matched.

The model bias for the rock stations, calculated as the logarithm (base 10) of the ratio of the observed to simulated Fourier spectra, averaged over 24 sites, is presented in Figure 4. The mean bias is within the 95% confidence limits of zero throughout almost the entire frequency range, showing that the adopted model adequately captures the spectral source and path effects and their spatial variability on average, relative to observations.

The ratio of the observed to synthetic spectrum as a function of distance is shown in Figure 5. As discussed earlier, this test checks the occurrence of any systematic distance-dependent bias, which could be due to inadequacies in modeling the path effect. Misfits at individual stations are shown for two representative frequencies of 0.7 and 2.0 Hz, where model bias is moderate. Figure 5 shows that the misfits appear to be randomly distributed around unity. All soil stations used are in the same hypocentral distance interval.

Calculation of Weak-Motion Responses at Soil Sites

In Taiwan, site class D includes fluvial terraces, stiff clays, and sandy gravel deposits (Lee *et al.*, 2001a). Weak-motion response for site class D was estimated using the spectral-ratio technique. We inspected the Chi-Chi aftershock datasets released so far (Lee *et al.*, 2001c,d) in order to find pairs of neighboring soil and rock sites that recorded the same aftershocks. Our selection criteria included a maximum distance of 10 km between the reference-rock and soil stations and a minimum number of three aftershocks recorded at both.

Sixteen soil sites satisfied these criteria. Their locations, relative to the corresponding reference station, are depicted in Figure 6. Table 3 presents station information, including station-to-fault distance measures, the distance between the soil and reference sites, the PHA recorded during the mainshock, and the number of aftershocks used in the estimation of each average weak-motion amplification function. The selected time windows started slightly before the *S*-wave arrival, and their duration varied depending on the source-

Table 2
Modeling Parameters

Parameter	Parameter value
Fault orientation (strike/dip)	5°/34°
Fault dimensions along strike and dip (km)	110 by 40
Depth of the upper edge of the fault (km)	0
Mainshock moment (dyne cm)	2.8×10^{27}
Subfault dimensions (km)	11×10
Stress parameter $\Delta\sigma$ (bar)	50
Radiation-strength factor	1.0
Number of subsources summed	40
$Q(f)$	$117 \cdot f^{0.77}$
Geometric spreading	$1/R$ for $R < 50$ km $1/R^0$ for 50 km $\leq R <$ 150 km $1/R^{0.5}$ for $R \geq 150$ km
Windowing function	Cosine-tapered boxcar
Kappa (sec)	0.07
Crustal amplification	Boore and Joyner (1997) western North America generic rock site
Crustal shear-wave velocity (km/sec)	3.2
Rupture velocity (km/sec)	0.8 × (shear-wave velocity)
Crustal density (g/cm^3)	2.7

station separation. For every observed trace analyzed, the geometric average of the spectra of the two horizontal components was taken. Prior to Fourier transformation, all windows were symmetrically tapered (at 5%) using a cosine function. In all waveforms the signal-to-noise ratio was at least 1–3 throughout the examined frequency range. The average empirical transfer functions estimated for these 16 sites (± 1 standard deviation of the data) are shown in Figure 7a. It is interesting to note the variability in both the amplification levels and resonance frequencies among the examined sites, although they all have been classified within the same site class (D).

In Figure 7b, we present the average transfer function, computed from the entire set of aftershock spectral ratios used to estimate the 16 site-specific responses. The suggested amplifications are comparable to the generic soil amplification proposed for the other regions, for example, for California (figure 1 of Beresnev, 2002, adapted from Silva *et al.*, 1997). This function is an estimate of the average site response (site class D) in Taiwan, although the individual site-response variability is large, as is reflected in the standard deviation in Figure 7b.

Simulation of Mainshock Records at Soil Sites: Implications for Nonlinearity

As a final step in our analysis, the calibrated model was combined with the weak-motion amplification functions to simulate the spectra at site class D. First, we applied the finite-fault code to the 16 sites for which we estimated site-specific response information. Each simulated spectrum was amplified by the site's empirical transfer function. This was the only difference in the input parameters in soil-site simulations compared with those used in the validation (Table 2). The kappa parameter was also fixed at its validated value of 0.07 sec, since any difference in kappa between soil and rock sites had already been included in the empirical transfer functions.

The average model bias for the 16 stations, normalized by the average rock-station bias, is presented in Figure 8a, where the dashed lines show $\pm 95\%$ confidence limits of the mean. As discussed in the Method section, this bias is an estimate of the average strong–to–weak-motion amplification ratio. An overprediction of the observed mainshock motions using the weak-motion amplification functions occurs throughout the entire frequency range. However, this result is at the boundary of statistical significance at the 95% confidence level. We also calculated the bias for several stations in Table 3 that showed the highest observed acceleration level (close to or exceeding 200 cm/sec^2). The resulting uncertainty was similar to that shown for all 16 sites in Figure 8a.

The number of soil stations with empirical weak-motion responses is only 16. This may have limited the possibility of obtaining statistically robust results, so we included more site class D stations in our simulations by assigning them the average site class D transfer function from Figure 7b. In this approach, the amplification in Figure 7b, estimated as the average of 82 aftershock spectral ratios, is considered to be representative of all class D sites in Taiwan. Despite the observed individual-response variability, these stations share similar geology (Lee *et al.*, 2001a) and can be expected to cluster around a common mean amplification curve.

The model bias for all 115 site class D stations in Taiwan that recorded the mainshock at hypocentral distances less than 120 km, corrected for the average rock-station bias, is presented in Figure 8b. Consistent with the results from the 16 soil stations, the predicted spectral level appears to be larger than the observations throughout the entire frequency range, with a small exception around 0.4 Hz. This

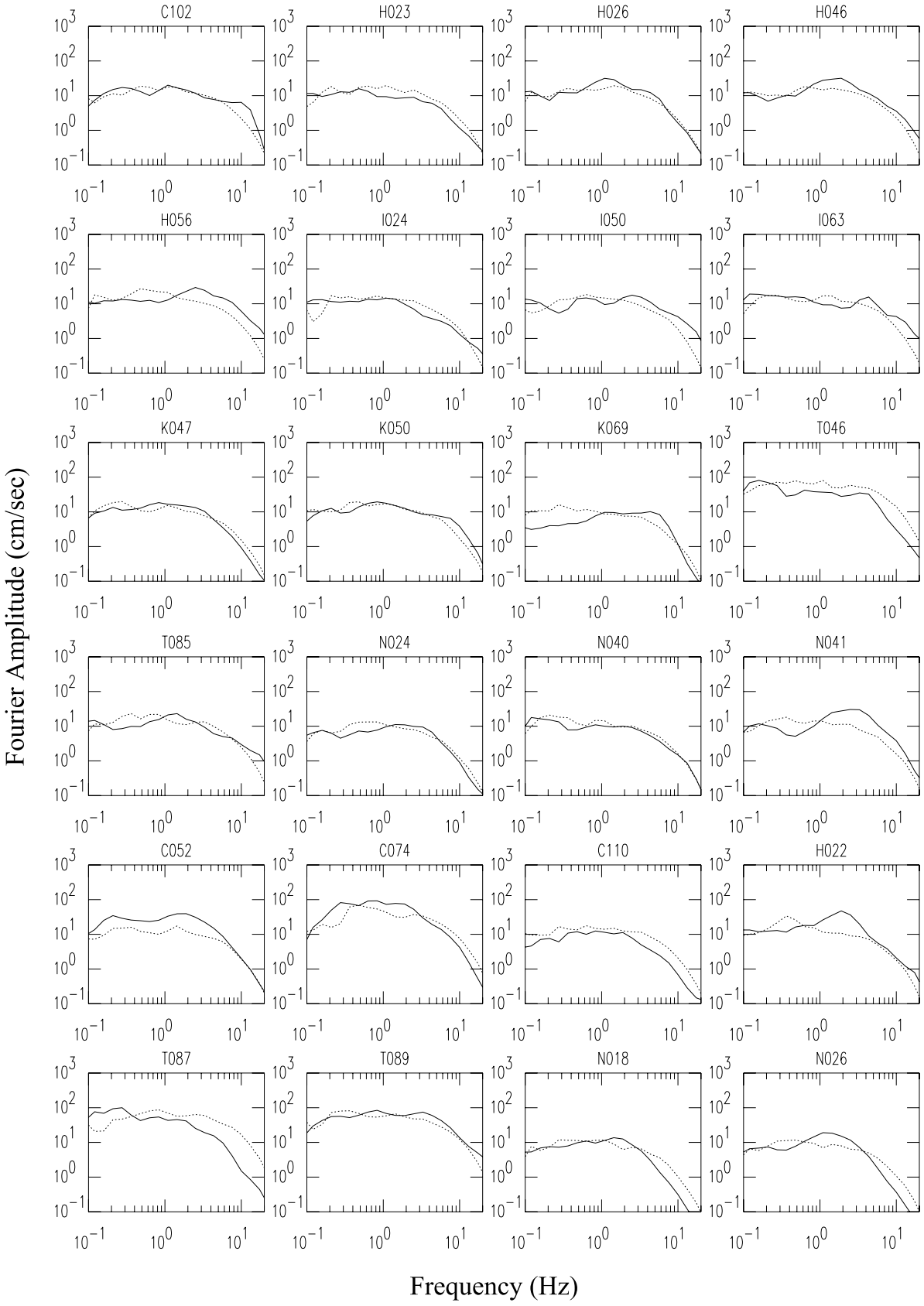

Figure 2. Comparison of observed (solid lines) and simulated (dashed lines) Fourier amplitude spectra of acceleration at 24 rock sites used in the calibration.

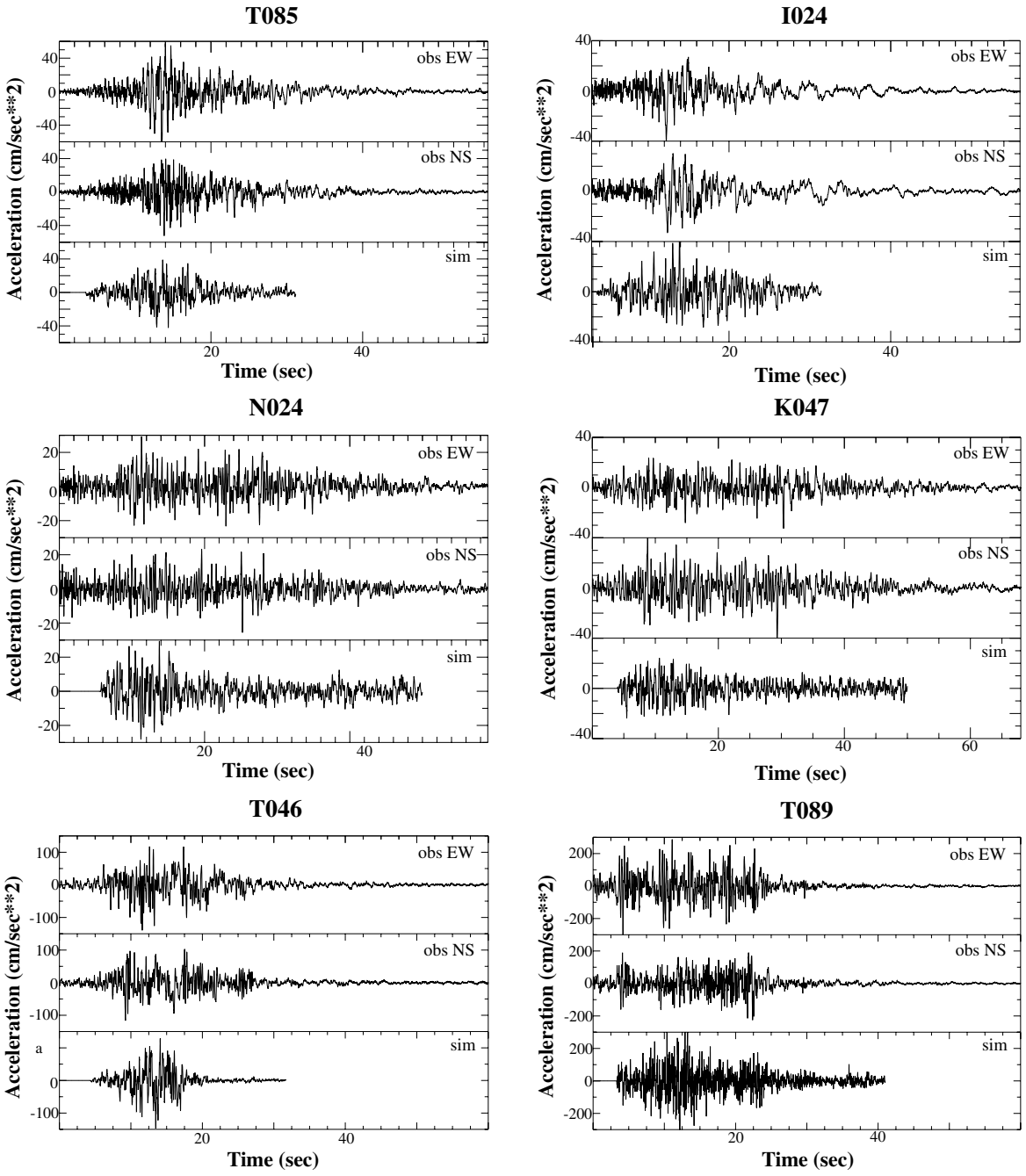

Figure 3. Comparison of observed east–west (top) and north–south (middle) acceleration components with the simulated random horizontal accelerogram (bottom) at six representative rock sites.

difference of the bias from zero is statistically significant at the 95% confidence level (except near 0.4 Hz).

Figure 9 plots the ratio of strong- to weak-motion amplification estimated at 115 sites as a function of synthetic peak acceleration at the base of soil. The results are shown for 2.5 Hz, where the maximum reduction in amplification is observed in Figure 8b. Significant scatter exists in the data, which is attributed to the uncertainties in modeling site-specific responses by the average transfer function, as well as in estimating PGA at the base of soil using the calibrated model. Despite the scatter, a weak trend is seen toward an overall decrease in the amplification ratio as the input acceleration level increases. The data corresponding to low PGA values cluster around unity, whereas at larger input levels ($\gtrsim$200–300 cm/sec^2) there seems to be a systematic tendency for the ratios to drop below unity. This result seems logical, since only the sites with the highest developed strain would normally primarily contribute to the observed nonlin-

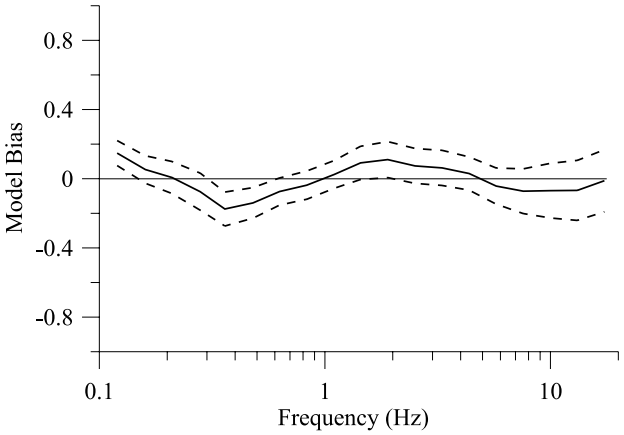

Figure 4. Bias of the calibrated model, showing the logarithm of the ratio of the observed to simulated spectrum, averaged over all 24 rock sites. The dashed lines indicate the 95% confidence interval of the mean.

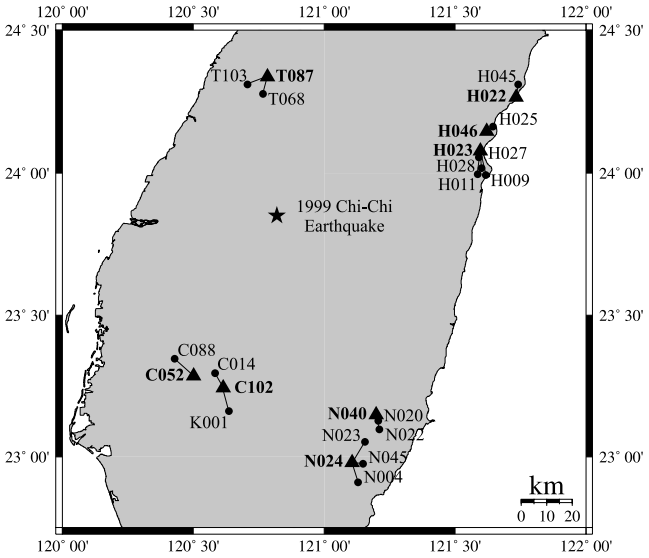

Figure 6. Locations of the stations used in the spectral-ratio analysis. The reference and soil stations are shown as triangles and circles, respectively. Each soil site is connected to its reference station by a straight line. The star indicates the epicenter of the mainshock.

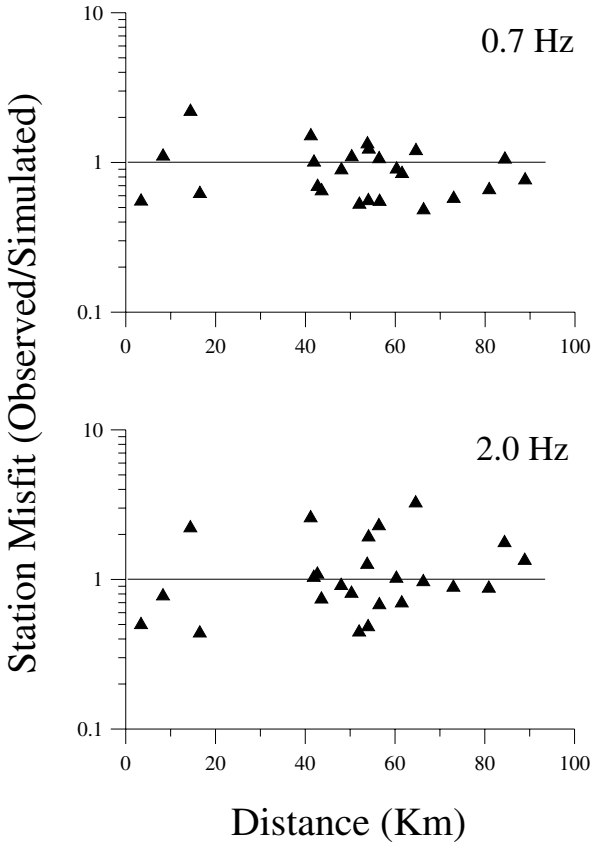

Figure 5. Station misfits (ratios of observed to simulated spectra) as a function of closest distance to the rupture plane. Misfits are shown for two representative frequencies of 0.7 and 2.0 Hz.

ear response; however, due to large individual-response variability, a statistically significant bias, such as that shown in Figure 8b, could only be obtained when all 115 stations were grouped together.

The reduction in amplification and the threshold acceleration level at which nonlinearity becomes detectable, suggested by Figures 8b and 9, are consistent with the recent studies of large California earthquakes (the 1987 Whittier Narrows, 1989 Loma Prieta, and 1994 Northridge events). For example, Beresnev *et al.* (1998a), Hartzell (1998), Su *et al.* (1998), and Beresnev (2002) reported PHAs of approximately 200–300 cm/sec^2, above which they observed a significant difference between the weak- and strong-motion amplifications. The data in Figure 9 are consistent with this value. Also, Figures 8b and 9 suggest that an overall reduction in amplification in strong motions to about 0.5–0.6 of that in weak motions could be expected. This value is also consistent with those obtained in previous studies. Beresnev (2002) reported a maximum reduction coefficient of 0.5–0.6 in the frequency range of 1–3 Hz, Field *et al.* (1997) gave a coefficient of 0.5 between approximately 1 and 6 Hz, and Beresnev *et al.* (1998a) reported a coefficient of 0.5 between 2 and 10 Hz. From the result in Figure 8b, the nonlinear response during the Chi-Chi event appears to have affected the wider frequency band, from 0.1 to 20 Hz. Su *et al.* (1998) and Hartzell (1998) also measured the behavior of strong–to–weak-motion amplification ratios averaged over broad frequency ranges (0.5–15 Hz and 0.75–10 Hz, respectively) and reported similar reductions.

Increased data volumes at high base PGA are required

Table 3
Information on 16 Soil Sites used in Spectral-Ratio Analyses

Station Code	Latitude (°)	Longitude (°)	Closest Distance to Rupture Plane (km)	Hypocentral Distance (km)	Distance from Reference Site (km)	PHA (cm/sec^2)	Number of Aftershocks
C014	23.296	120.583	37.2	66.3	6.2	255	8
C088	23.346	120.429	40.0	68.3	9.8	207	9
H009	23.993	121.617	55.2	84.5	9.8	101	3
H011	23.996	121.586	52.1	81.5	9.3	97	3
H025	24.163	121.645	56.4	92.3	2.2	67	5
H027	24.055	121.591	51.7	83.4	3.1	121	3
H028	24.017	121.601	53.2	83.5	7.3	101	3
H045	24.310	121.741	65.2	107.8	4.4	186	4
K001	23.162	120.636	50.7	79.2	9.6	43	6
N004	22.910	121.129	79.8	110.5	7.0	43	4
N020	23.127	121.206	59.1	91.2	3.1	35	6
N022	23.097	121.211	62.2	94.4	6.2	74	6
N023	23.053	121.156	65.3	96.5	9.8	66	4
N045	22.976	120.583	73.2	66.3	3.1	39	4
T068	24.277	120.766	3.1	46.3	7.6	502	7
T103	24.310	120.707	2.4	50.7	7.6	149	7

The number of aftershocks used for the derivation of each individual transfer function is given in the last column.

to make a more robust determination of the nonlinearity "threshold." Figure 9 emphasizes a general difficulty in quantitative studies of nonlinear site response, that is, the natural paucity of recorded data at very high acceleration levels. Even for a large-magnitude event, recorded by one of the densest strong-motion networks in the world, such as the 1999 Chi-Chi event, there are only four site class D stations at which the estimated base peak acceleration exceeded 300 cm/sec^2. More accurate conclusions could also be made as more data from the enormous aftershock database, recorded following the mainshock, are released. Having the site-specific response information at more than 16 stations could significantly improve the accuracy of the estimation of the site-specific difference between strong- and weak-motion amplifications, such as shown in Figure 8a.

Conclusions

The stochastic finite-fault technique for modeling ground motions was applied to the devastating 1999 Chi-Chi earthquake. As a first step, we calibrated the finite-fault model against 24 rock stations located at various azimuths around the fault. Despite the simplicity of the method, it provided an accurate prediction of the observed Fourier amplitude spectra on average, in line with the results of previous method validations performed for other events around the world. The model was also unbiased with respect to distance up to about 120 km using a Taiwan path-effect model. The rock-site calibration provided an unusually low value of the radiation-strength factor s, a parameter controlling the level of high-frequency radiation and determining the maximum slip velocity on the fault. This result suggests the lower-than-usual slip velocities during the Chi-Chi event, resulting in atypically low ground-motion levels for an event of magnitude M 7.6, also reported in several earlier studies.

The calibrated model was used to simulate acceleration spectra at site class D stations located within the same distance range. The simulated spectra were amplified by the site-response functions determined empirically from aftershock data. The method was initially applied to the 16 soil sites with known site-specific response information. An average empirical transfer function was also computed and applied to the entire set of 115 soil stations.

Due to large interstation response variability and a relatively small number of stations involved, we were unable to derive a statistically significant difference in weak- and strong-motion amplifications based on the site-specific responses available at 16 stations. However, the average amplification ratio calculated for the 115 stations, with the mean site class D transfer function assigned to all of them, showed a statistically significant reduction in amplification. In this case, the analysis benefited from the fact that the individual site-response variability averaged out to smaller overall uncertainty when a much greater number of stations were considered. This shows that the responses of all 115 sites, sharing similar site classification, were still well represented on average by the mean empirical transfer function. Based on Figure 8b, the amplification reduction occurred in almost the entire frequency band of the analysis from 0.1 to 20 Hz, to a maximum of 0.5–0.6 of the weak-motion amplification. The "onset" of detectable nonlinearity lies roughly above input accelerations of 200–300 cm/sec^2. Both the value of overall amplification reduction and the threshold level for detectable nonlinearity agree with previous studies of the average characteristics of nonlinearity.

Although Figures 8b and 9 reveal observable nonlinear

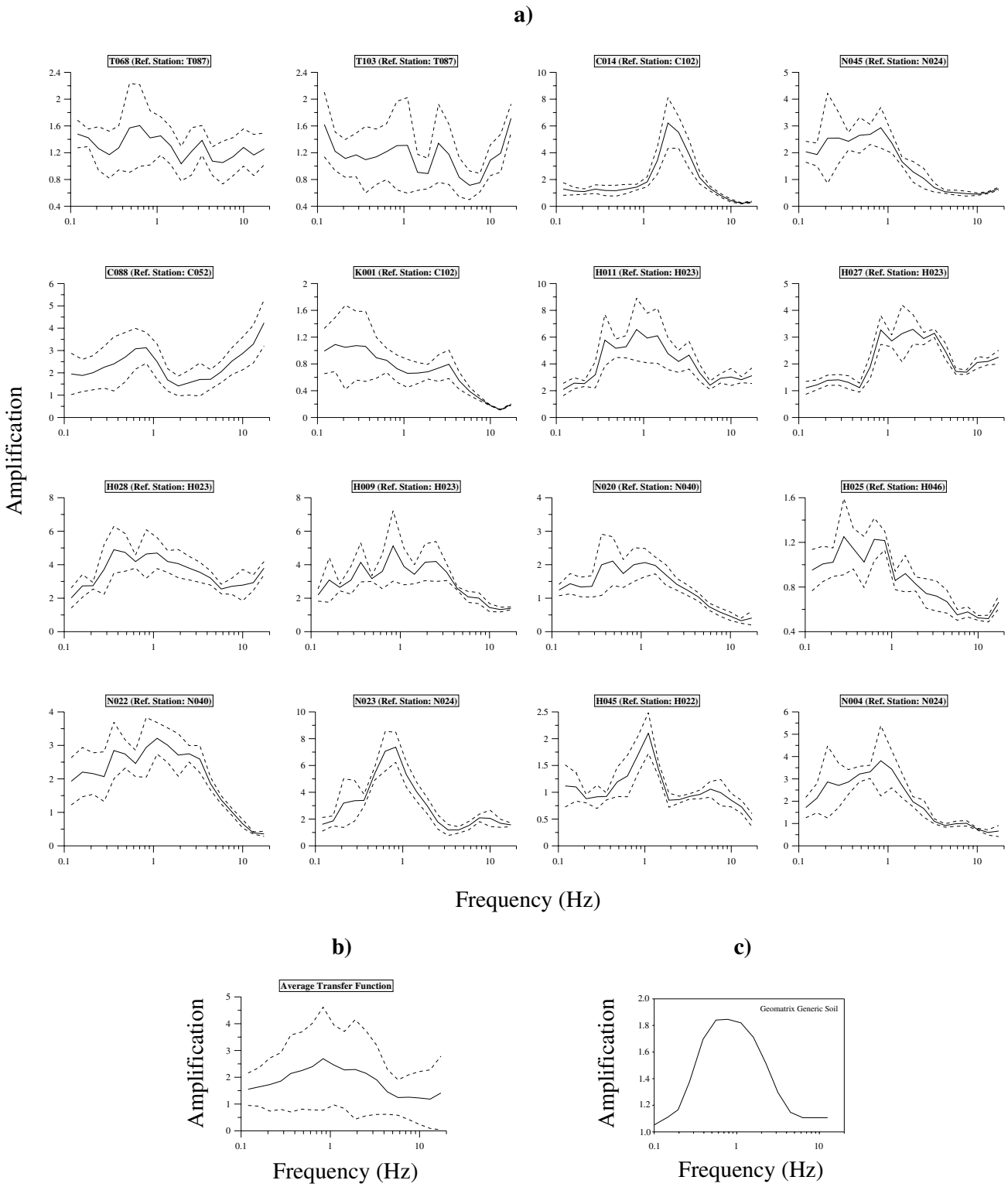

Figure 7. Soil-station average transfer functions estimated using the spectral-ratio technique. (a) Individual transfer functions at the 16 site class D sites. The names of the site and the corresponding reference station (in parentheses) are given at the top of each plot. (b) Average transfer function for the 16 sites. The dashed lines correspond to ± 1 standard deviation of the data. (c) Mean linear transfer function for Geomatrix generic "soil" (classes C–D), relative to generic "rock" (classes A–B) (after Silva *et al.*, 1997).

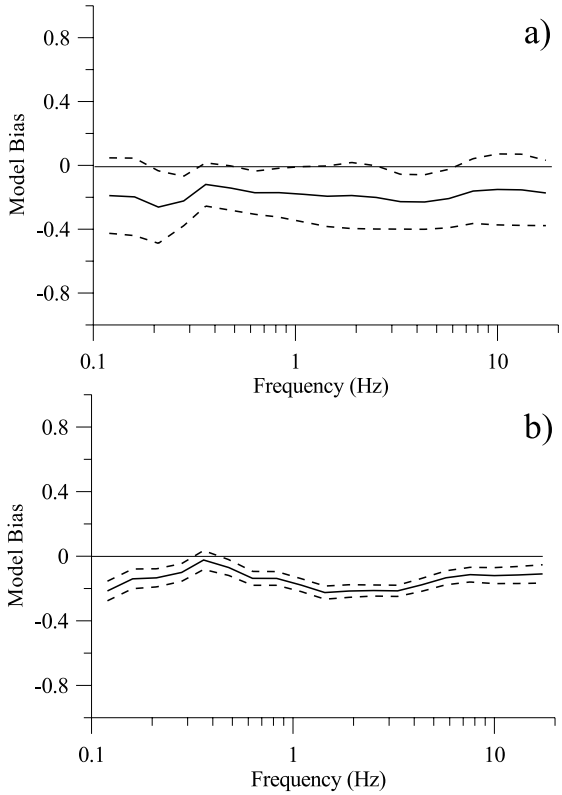

Figure 8. Model bias for soil-site simulations, normalized by rock-station prediction bias (Fig. 4). (a) Bias for 16 soil sites, for which simulated spectra were amplified by the site-specific weak-motion transfer functions. (b) Bias for 115 soil sites, for which the average class D empirical transfer function was used to amplify the synthetic spectra.

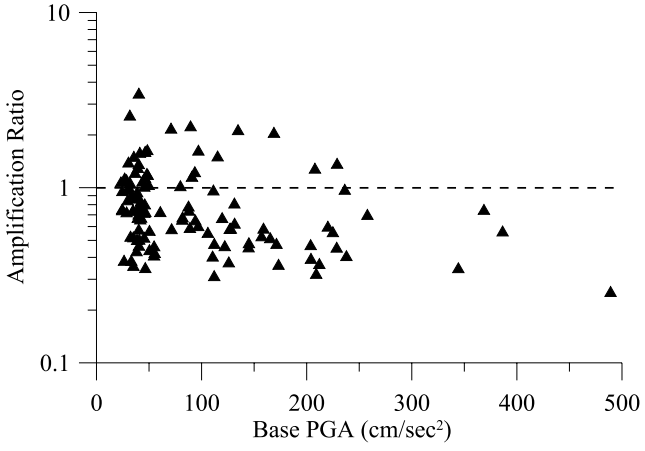

Figure 9. Ratios of strong- to weak-motion amplification at individual D sites islandwide as a function of estimated base peak acceleration. The ratios are shown at the frequency of 2.5 Hz.

phenomena during the Chi-Chi mainshock, the picture is not as informative as one could expect it to be from the wealth of strong-motion records that this earthquake provided. This is primarily due to the relatively small amount of aftershock data released so far, which does not allow detailed examination of soil response at a large number of site class D stations or any of the site class E ("soft soil") stations characterized by even lower near-surface velocities. Future releases of additional aftershock records could help enhance the quantitative character of our conclusions, to draw as many lessons as possible from the catastrophic Chi-Chi event about the characteristics of nonlinear soil response in the near field of large earthquakes.

Acknowledgments

This work was supported by the U.S. Geological Survey (USGS), Department of the Interior, under USGS Award Number 02HQGR0052. The views and conclusions contained in this document are those of the authors and should not be interpreted as necessarily representing the official policies, either expressed or implied, of the U.S. government. This study would not be possible without generous help from William H. K. Lee, who provided us with up-to-date strong-motion datasets of the Chi-Chi mainshock, as well as invaluable aftershock data soon after their release. The article benefited from careful reviews by L. F. Bonilla and an anonymous reviewer. The finite-fault radiation simulation code FINSIM, along with copies of all input files, is available from the authors upon request.

References

Aki, K. (1993). Local site effects on weak and strong ground motions, *Tectonophysics* **218,** 93–111.

Anderson, J. G., and S. E. Hough (1984). A model for the shape of the Fourier amplitude spectrum of acceleration at high frequencies, *Bull. Seism. Soc. Am.* **74,** 1969–1993.

Berardi, R., M. J. Jiménez, G. Zonno, and M. García-Fernández (2000). Calibration of stochastic finite-fault ground motion simulations for the 1997 Umbria–Marche, central Italy, earthquake sequence, *Soil Dyn. Earthquake Eng.* **20,** 315–324.

Beresnev, I. A. (2002). Nonlinearity at California generic soil sites from modeling recent strong-motion data, *Bull. Seism. Soc. Am.* **92,** 863–870.

Beresnev, I. A., and G. M. Atkinson (1998a). FINSIM: a FORTRAN program for simulating stochastic acceleration time histories from finite faults, *Seism. Res. Lett.* **69,** 27–32.

Beresnev, I. A., and G. M. Atkinson (1998b). Stochastic finite-fault modeling of ground motions from the 1994 Northridge, California, earthquake. I. Validation on rock sites, *Bull. Seism. Soc. Am.* **88,** 1392–1401.

Beresnev, I. A., and G. M. Atkinson (2001). Subevent structure of large earthquakes: a ground motion perspective, *Geophys. Res. Lett.* **28,** 53–56.

Beresnev, I. A., and G. M. Atkinson (2002). Source parameters of earthquakes in eastern and western North America based on finite-fault modeling, *Bull. Seism. Soc. Am.* **92,** 695–710.

Beresnev, I. A., and K.-L. Wen (1996). Nonlinear soil response: a reality? *Bull. Seism. Soc. Am.* **86,** 1964–1978.

Beresnev, I. A., G. M. Atkinson, P. A. Johnson, and E. H. Field (1998a). Stochastic finite-fault modeling of ground motions from the 1994 Northridge, California, earthquake. II. Widespread nonlinear response at soil sites, *Bull. Seism. Soc. Am.* **88,** 1402–1410.

Beresnev, I. A., E. H. Field, K. Van Den Abeele, and P. A. Johnson (1998b). Magnitude of nonlinear sediment response in Los Angeles basin during the 1994 Northridge, California, earthquake, *Bull. Seism. Soc. Am.* **88,** 1079–1084.

Boore, D. M., and W. B. Joyner (1997). Site amplifications for generic rock sites, *Bull. Seism. Soc. Am.* **87,** 327–341.

Campbell, K. W., and Y. Bozorgnia (2003). Updated near-source ground motion (attenuation) relations for the horizontal and vertical components of peak ground acceleration and acceleration response spectra, *Bull. Seism. Soc. Am.* **93,** 314–331.

Castro, R. R., A. Rovelli, M. Cocco, M. Di Bona, and F. Pacor (2001). Stochastic simulation of strong-motion records from the 26 September 1997 (M_w 6), UmbriaMarche (central Italy) earthquake, *Bull. Seism. Soc. Am.* **91,** 27–39.

Chang, G., Y. M. Wu, and T. C. Shin (2000). Relocating the 1999 Chi-Chi Earthquake, Taiwan, *TAO* **11,** 581–590.

Chen, K. C., T. C. Shin, and J. H. Wang (1989). Estimates of coda Q in Taiwan, *Proc. Geol. Soc. China* **32,** 339–353.

Chi, W.-C., D. Dreger, and A. Kaverina (2001). Finite-source modeling of the 1999 Taiwan (Chi-Chi) earthquake derived from a dense strong-motion network, *Bull. Seism. Soc. Am.* **91,** 1144–1157.

Cultrera, G., D. M. Boore, W. B. Joyner, and C. M. Dietel (1999). Nonlinear soil response in the vicinity of the Van Norman Complex following the 1994 Northridge, California, earthquake, *Bull. Seism. Soc. Am.* **89,** 1214–1231.

Das, S., and B. V. Kostrov (1994). Diversity of solutions of the problem of earthquake faulting inversion: application to *SH* waves for the great 1989 Macquarie Ridge earthquake, *Phys. Earth Planet. Interiors* **85,** 293–318.

Delouis, B. D. Giardini, P. Lundgren, and J. Salichon (2002). Joint inversion of InSAR, GPS, teleseismic, and strong-motion data for the spatial and temporal distribution of earthquake slip: application to the 1999 Izmit mainshock, *Bull. Seism. Soc. Am.* **92,** 278–299.

Dimitriu, P. P. (2002). The HVSR technique reveals pervasive nonlinear sediment response during the 1994 Northridge earthquake (M_w 6.7), *J. Seism.* **6,** 247–255.

Dimitriu, P., N. Theodulidis, and P.-Y. Bard (2000). Evidence of nonlinear site response in HVSR from SMART1 (Taiwan) data, *Soil Dyn. Earthquake Eng.* **20,** 155–165.

Erdik, M., and E. Durukal (2003). Simulation modeling of strong ground motion, in *Earthquake Engineering Handbook*, W. F. Chen and C. Scawthorn (Editors), CRC Press, Boca Raton, Florida, 6-16-67.

Field, E. H., P. A. Johnson, I. A. Beresnev, and Y. Zeng (1997). Nonlinear ground-motion amplification by sediments during the 1994 Northridge earthquake, *Nature* **390,** 599–602.

Field, E. H., S. Kramer, A.-W. Elgamal, J. D. Bray, N. Matasovic, P. A. Johnson, C. Cramer, C. Roblee, D. J. Wald, L. F. Bonilla, P. P. Dimitriu, and J. G. Anderson (1998a). Nonlinear site response: where we're at, *Seism. Res. Lett.* **69,** 230–234.

Field, E. H., Y. Zeng, P. A. Johnson, and I. A. Beresnev (1998b). Nonlinear sediment response during the 1994 Northridge earthquake: observations and finite-source simulations, *J. Geophys. Res.* **103,** 26,869–26,883.

Hartzell, S. (1998). Variability in nonlinear sediment response during the 1994 Northridge, California, earthquake, *Bull. Seism. Soc. Am.* **88,** 1426–1437.

Hartzell, S., S. Harmsen, A. Frankel, and S. Larsen (1999). Calculation of broadband time histories of ground motion: comparison of methods and validation using strong ground motion from the 1994 Northridge earthquake, *Bull. Seism. Soc. Am.* **89,** 1484–1504.

Hough, S. E., S. Martin, R. Bilham, and G. M. Atkinson (2002). The 26 January 2001 M 7.6 Bhuj, India earthquake: observed and predicted ground motions, *Bull. Seism. Soc. Am.* **92,** 2061–2079.

Iglesias, A., S. K. Singh, J. F. Pacheco, and M. Ordaz (2002). A source and wave propagation study of the Copalillo, Mexico, earthquake of 21 July 2000 (M_w 5.9): implications for seismic hazard in Mexico City from inslab earthquakes, *Bull. Seism. Soc. Am.* **92,** 1060–1071.

Ishihara, K. (1996). *Soil Behaviour in Earthquake Geotechnics*, Clarendon, London, 350 pp.

Lee, C.-T., C.-T. Cheng, C.-W. Liao, and Y.-B. Tsai (2001a). Site classification of Taiwan free-field strong-motion stations, *Bull. Seism. Soc. Am.* **91,** 1283–1297.

Lee, W. H. K., T. C. Shin, K. W. Kuo, K. C. Chen, and C. F. Fu (2001b). CWB free-field strong-motion data from the 21 September Chi-Chi, Taiwan, earthquake, *Bull. Seism. Soc. Am.* **91,** 1370–1376.

Lee, W. H. K., T. C. Shin, and C. F. Wu (2001c). Free-field strong-motion data from 30 early aftershocks of the 1999 Chi-chi earthquake, Seismological Observation Center, Central Weather Bureau, Taipei, Taiwan (CD-ROM).

Lee, W. H. K., T. C. Shin, and C. F. Wu (2001d). Free-field strong-motion data from three major aftershocks of the 1999 Chi-chi earthquake, Seismological Observation Center, Central Weather Bureau, Taipei, Taiwan (CD-ROM).

Ma, K.-F., J. Mori, S.-J. Lee, and S. B. Yu (2001). Spatial and temporal distribution of slip for the 1999 Chi-Chi, Taiwan, earthquake, *Bull. Seism. Soc. Am.* **91,** 1069–1087.

Olson, A. H., and J. G. Anderson (1988). Implications of frequency-domain inversion of earthquake ground motions for resolving the space-time dependence of slip on an extended fault, *Geophys. J.* **94,** 443–455.

Ou, G.-B., and R. B. Herrmann (1990). A statistical model for ground motion produced by earthquakes at local and regional distances, *Bull. Seism. Soc. Am.* **80,** 1397–1417.

Roumelioti, Z., and A. Kiratzi (2002). Stochastic simulation of strong-motion records from the 15 April 1979 (**M** 7.1) Montenegro earthquake, *Bull. Seism. Soc. Am.* **92,** 1095–1101.

Silva, W. J., N. Abrahamson, G. Toro, and C. Costantino (1997). Description and Validation of the Stochastic Ground Motion Model, report to Brookhaven National Laboratory, Associated Universities, Inc., Upton, New York.

Singh, S. K., B. K. Bansal, S. N. Bhattacharya, J. F. Pacheco, R. S. Dattatrayam, M. Ordaz, G. Suresh, Kamal, and S. E. Hough (2003). Estimation of ground motion for Bhuj (26 January, 2001; M_w 7.6) and for future earthquakes in India, *Bull. Seism. Soc. Am.* **93,** 353–370.

Sokolov, V. (2000). Spectral parameters of ground motion in different regions: comparison of empirical models, *Soil Dyn. Earthquake Eng.* **19,** 173–181.

Su, F., J. G. Anderson, and Y. Zeng (1998). Study of weak and strong ground motion including nonlinearity from the Northridge, California, earthquake sequence, *Bull. Seism. Soc. Am.* **88,** 1411–1425.

Wang, W.-H., S-H. Chang, and C.-H. Chen (2001). Fault slip inverted from surface displacements during the 1999 Chi-Chi, Taiwan, earthquake, *Bull. Seism. Soc. Am.* **91,** 1167–1181.

Wu, C., M. Takeo, and S. Ide (2001). Source process of the Chi-Chi earthquake: a joint inversion of strong motion data and global positioning system data with a multifault model, *Bull. Seism. Soc. Am.* **91,** 1128–1143.

Zeng, Y., and C.-H. Chen (2001). Fault rupture of the 20 September 1999 Chi-Chi, Taiwan, earthquake, *Bull. Seism. Soc. Am.* **91,** 1088–1098.

Department of Geophysics
Aristotle University of Thessaloniki
P.O. Box 352-1
54006 Thessaloniki, Greece
zroum@lemnos.geo.auth.gr
(Z.R.)

Department of Geological and Atmospheric Sciences
Iowa State University
253 Science I
Ames, Iowa 50011-3212
beresnev@iastate.edu
(I.A.B.)

Manuscript received 1 November 2002.